Current understanding of tokamak plasma eruption control and the consequences for ITER

Joe Allen, JOA509

24th May 2016

Abstract

The background of edge localised modes (ELMs), theoretical bases of different methods of their control and ways they are put into practice are reviewed in this article, along with a short discussion of alternative modes of tokamak operation. ELMs are a generic feature of tokamak H-mode operation and their detrimental effect on density and energy confinement, along with first wall component lifetime, means that their control is key for successful operation of ITER. Three main ELM control methods are discussed; resonant magnetic perturbations, pellet injection and vertical kicks. Positives and drawbacks of each technique are examined, specifically in view of their domain of utility on ITER. Progress in controlling these ubiquitous H-mode plasma eruptions has come a long way and been rapidly developed by global collaborations; however, more groundwork is required to ensure the safe extrapolation of these control schemes to all ITER scenarios.

Contents

1 Background

Since their experimental observation over thirty years ago [1], edge localised modes (ELMs) have attracted a large amount of research interest. Toroidal magnetic field devices looking to maximise power production must operate in the high confinement regime (H-mode), in which the central plasma density profile is raised up on a pedestal, providing enhanced confinement [2]. This elevation is caused by a steep pressure gradient in the separatrix (the boundary between open and closed field lines at the edge of the plasma). Due to the unstable nature of this gradient, ELMs periodically disrupt the edge plasma, causing energy and particle losses; ELMs are a type of magnetohydrodynamic (MHD) instability [3]. There are several types of ELMs, type I ELMs are the main subject of this review.

In H-mode, type I ELMs are initiated when the pressure increases such that it reaches the ideal peeling-ballooning (PB) stability boundary, the manner of this cyclic process is shown in figure 1. This model was proposed in 2002 [4] and has since been developed and corroborated with experimental evidence [5]. More specifically, the high edge pressure gradient drives a large bootstrap current in the region which in turn produces $n \sim 3-30$ modes [6] which lead to eruptions from the plasma edge. The edge plasma rapidly collapses as the PB boundary is crossed; this collapse is due to the non-linear growth of MHD instabilities [7] that is observed when the edge pressure and current values near the two stability limits. Differing combinations of edge pressure and edge current density drive different modes unstable, table 1 shows the three main combinations for type I ELMs, which are naturally caused when the PB boundary is breached.

Table 1: The different instability modes resulting from combinations of pedestal pressure, p_{ped}, and current J_{ped}.[8]

p_{ped}	J_{ped}	**Mode**
High	Low	Ballooning
Low	High	Peeling
High	High	Peeling-ballooning

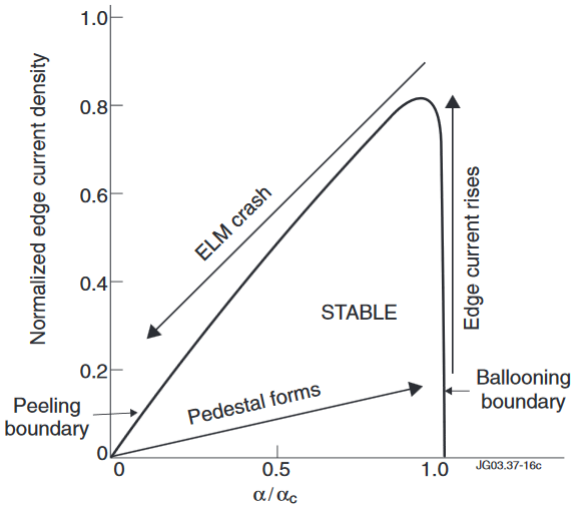

Figure 1: A pressure-current pathway followed throughout an ELM cycle [10]. An ELM is initiated when the peeling stability boundary is passed in the top right corner, returning the edge to a low pressure, low current state in the bottom left corner. The edge pressure is then built up quite rapidly to the ballooning limit by heating, compared to the edge current which increases more slowly, on a resistive timescale, until the crash. The edge pressure rests at the ballooning limit until the current increases across the peeling limit. Normalised edge pressure is on the x-axis.

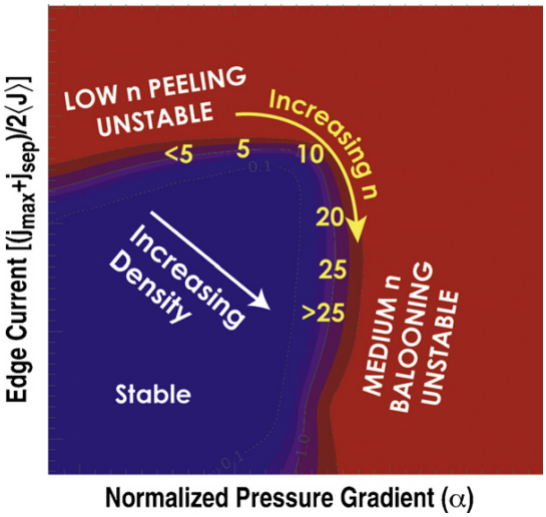

Figure 2: Edge current-pressure peeling-ballooning boundary diagram, the values of n on the boundary estimate the most unstable toroidal mode number at that location [11].

There are several reasons why research into ELMs is so important and widespread. Perhaps most importantly, they initiate sudden bursts of heat flux onto the divertor region and plasma facing components (PFCs) which can cause rapid decay of tokamak lifetime when these fluxes are unreasonably high. This has a knock-on effect on the sputtering of PFC materials into the plasma, hence ELMs contribute quite heavily to core plasma impurity accumulation. They, type I ELMs certainly, degrade plasma energy confinement which is undesirable for the competitiveness of fusion in the energy market. In addition, Hill [9] asserts that ELMs widen the density profile in the scrape-off layer (SOL).

Level of plasma shaping has a drastic effect on the size of the stable region below the PB limit, which can be seen in figure 3, an example being that increased triangularity extends the stable region to encompass higher edge pressure and current values [8]. Different modes are more likely to be driven unstable depending on the toroidal mode number, n, of the current perturbation. Figure 2 pictorially shows the location of different values of n on the PB stability boundary.

Current understanding is that ELMs of different magnitudes are produced depending on which stabil-

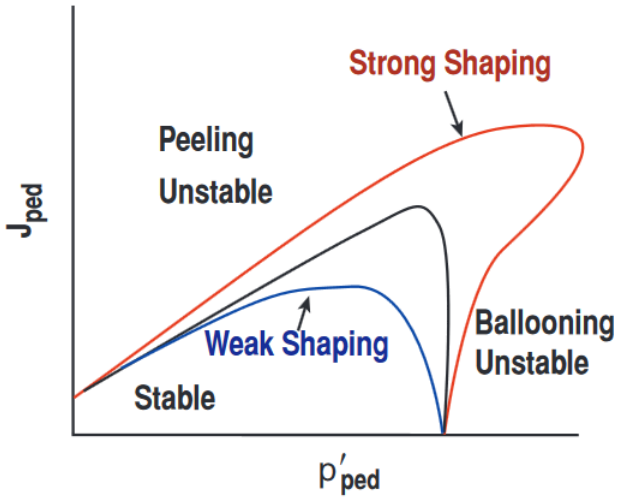

Figure 3: Differing peeling-ballooning stability boundaries for varying degrees of plasma shaping [12]. The plasma can be shaped (mainly) by vertical elongation or triangulation. No shaping gives a circular cross section.

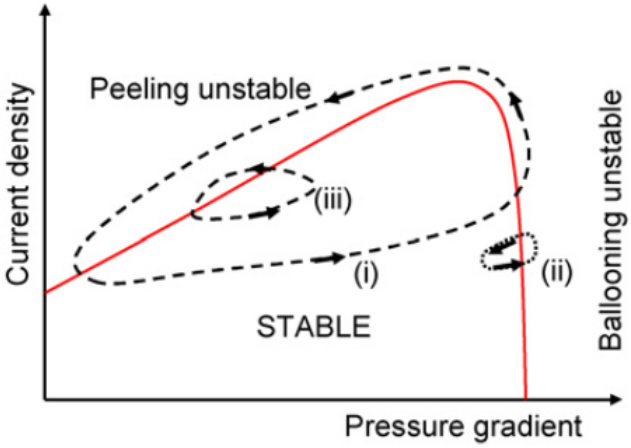

Figure 4: (i) Qualitative ELM cycle pathways: peeling-ballooning limit breached causes a large type I ELM; (ii) ballooning limit breached, produces either small ELMs or none at all; (iii) peeling limit breached causes a small ELM [13].

ity boundary is infringed, visualised in figure 4. The possibility of no ELMs being produced in case (ii) is a result of the fact that the enhanced transport due to the breach reduces the edge pressure gradient, which prevents an eruption [13].

Despite the many negative effects of ELMs on reactor lifetime, they do drive some positive processes such as enhanced transport, which reduces impurity fraction in the bulk plasma. As a result of this, a controlled amount of low power ELMs may be desirable to keep the core clean and give the ability to control the plasma density [9]. The positive impact of this impurity removal is greater than the resulting drop in fusion performance due to loss of energy confinement [14]. Edge-plasma eruptions can easily be viewed by measuring the corresponding peak in H_α emission at the eruption position [9].

Type-I ELMs produce uneven heat loads on the inner and outer divertor plates. Observations on JET (the Joint European Torus) and ASDEX Upgrade (AUG) found that the maximum heat flux asymmetry leads to twice the flux on the inner plate compare to the outer plate [15].

Several tokamaks have corroborated the scaling of ELM frequency given in equation 1 [16, 17], showing that is possible to decrease the time between ELMs in order to reduce their magnitude. P_{SOL} is essentially fixed for a given machine and is estimated to be approximately 100 MW in ITER [18].

$$f_{ELM}\Delta W_{ELM} = (0.2 - 0.4)P_{SOL} \qquad (1)$$

Edge plasma collisionality has a distinct effect on the rate of ELMs. Decreasing collisionality reduces edge current density, allowing the plasma profile to remain below the peeling stability limit and thus suppress ELMs [19]. In other words, lowering collisionality, ν^*, causes the pressure cycle to retreat from the unstable peeling-ballooning region and thus leads to complete type I ELM suppression [20]. The pedestal pressure gradients drive bootstrap current in the edge, which adds to the edge current densities [8]. Edge collisionality has an important role in the effectiveness of ELM control, when using resonant magnetic perturbation (RMP - an ELM control method discussed in more detail in section 3.1) coils it can be the deciding factor between ELM suppression and mitigation [19]. Suppression is complete removal of ELMs, whereas mitigation is when their frequency is increased (causing a corresponding decrease in power due to equation 1.

The structure of this review is as follows: in section 2, the predicted difficulties for operation of ITER as a result of ELMs are discussed. In section 3, methods for ELM suppression and mitigation are summarised (specifically resonant magnetic perturbations, pellet injection and vertical kicks) and comments are made regarding their future implementation and effectiveness on ITER. Finally, section 4 briefly looks at alternative operating modes for tokamaks and section 5 includes suggestions for further work required in order to operate ITER in ELM suppressed or mitigated scenarios.

2 Problems for ITER

High heat fluxes expunged from the plasma by ELMs onto the first wall of a tokamak, operating in H-mode, may have disastrous consequences for a machine the size of ITER [14], as well as generally degrading particle and energy confinement. Moreover, there is a possibility that ELMs of large magnitude could destabilise core MHD modes, leading to deconstruction of internal transport barriers [21] (and to core impurity accumulation), or further loss of confinement.

A limit has been set on the maximum power fluxes allowed onto the PFCs in ITER, specifically half that which would melt these components [22]. Natural ELM frequency for ITER will be about 1 Hz [22] and the resultant power load on the PFCs will cause them and the tungsten (W) divertor plates to melt [23]. ITER will not be able to stand even one ELM of this magnitude and so it must operate in a completely ELM-mitigated regime [24]. Current research

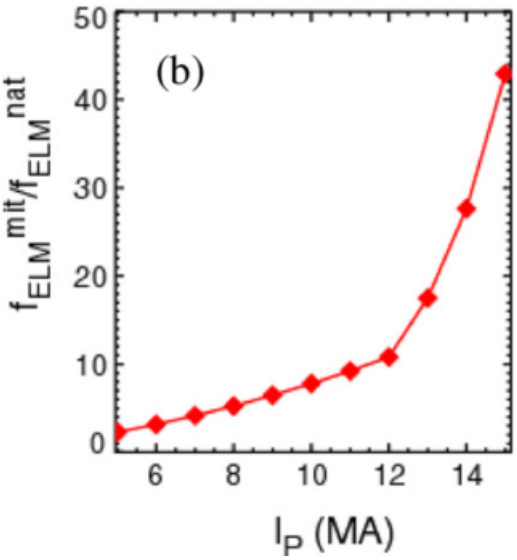

Figure 5: The required ratio of mitigated to natural ELM frequency to safeguard the performance for both a single discharge, keeping W impurity levels sufficiently low, and for the long term of ITER [19].

tokamaks are able to derive the parameters for ELM suppression and mitigation while running at regular operating power. ITER is simply too powerful and thus does not have this luxury.

ITER will be able to tolerate ELM energies of under 1 MJ per eruption; given that a single ELM can release a small fraction of the entire plasma energy, estimated to be up to around 20% of the pedestal plasma energy [25], this unwanted output must be reduced. Thus, a natural type I ELM in ITER could release 20 MJ in 500 μs [24], which is an unfeasibly high heat flux for the device. ITER is designed to operate at $I_p = 15$ MA and $Q_{DT} = 10$; however, if it lacks the necessary ability to control ELMs, the divertor and PFCs will start to degrade faster than desirable at plasma currents of $6 - 9$ MA [8]. Extended operation in the designed scenario would then not be possible.

Predictions have been drawn from analysis of data from current machines as to the maximum ELM energy flux impacting the divertor which does not significantly impact its lifetime: for the design scenario above ($I_p = 15$ MA, $Q_{DT} = 10$) this is approximately 0.5 MJ m^{-2} [26]. ITER is expected to have a natural ELM frequency of around 1 Hz [24] and there are estimated to be between $500 - 1000$ ELMs per shot in the $Q_{DT} = 10$ scenario. If each ELM in this operating scenario causes a degradation of 0.1μm in an area of the W divertor (an optimistic estimate), the capability of ITER will be reduced to less than thirty days of operation or a maximum of 100 shots [8] (assuming four discharges per day). With a cost exceeding 100 M€ [27] and a long period of enforced downtime during replacement, the collaboration cannot afford to render the divertor useless so quickly.

Another import factor is the ELM divertor footprint - the area of energy deposition on the divertor plates - which has been shown to decrease with decreasing ΔW_{ELM} [28]. While being beneficial for uncontrolled natural ELMs, this somewhat reduces the effectiveness of increasing f_{ELM}, regarding equation 1, as the heat flux incident on the divertor will not fall indefinitely with decreasing ΔW_{ELM} due to the divertor footprint becoming very small. The ratio $E_{inner}/E_{outer} \approx 2$ [15] of the asymmetry of ELM heat flux deposition on the inner and outer divertor plates further exacerbates this problem. This fact means that the threshold power dumped out of the plasma by ELMs on ITER must be further reduced to prevent the inner divertor degrading at too high a rate.

The maximum allowed energy flux per ELM of 0.5 MJ m^{-2} can be translated into a maximum loss of energy by the plasma per ELM which, when calculated gives $\Delta W_{ELM} = 0.66$ MJ[29]. This limit requires a thirty fold decrease in ELM energy from the natural ΔW_{ELM} of 20 MJ. There is a limit on the minimum ELM frequency necessary for ITER's operation due to the need to remove impurities [22], unless other methods of enhancing transport can be utilised. Figure 5 displays the dependence of this frequency ratio on the plasma current, I_p, at the minimum rate required to prevent catastrophic impurity accumulation in the core plasma.

3 Methods for ELM control

3.1 Resonant Magnetic Perturbations (RMPs)

RMP ELM control seeks to influence the edge plasma so as to hold it below the PB stability limit throughout the discharge. If the edge pressure can be maintained just under this limit, type I ELMs will not be triggered; this is very beneficial to the overall fusion performance of the machine, as the core plasma will remain at an optimally high pressure. If the transport rate in the edge transport barrier (ETB) can be augmented through external influence, the plasma pressure can be made to level off below the critical PB stability boundary.

Plasma density and confinement are reduced by around 10% by the use of RMP coils [8]; nevertheless, researchers using AUG saw a factor 6 reduction in

core plasma energy loss in ELM-mitigated shots with $n_{RMP} = 2$ toroidal edge perturbations [30]. Again on AUG, pellet injection was used to combat the density reduction in ELM mitigated regimes and also to bring the edge density above the threshold level necessary to reach said ELM mitigated regime [31]. There appears to exist a minimum edge plasma density below which ELM mitigation will not occur [30], hence pellet injection will need to be used in tandem with RMP control in ITER in order to keep the edge density above this threshold throughout the duration of a shot.

DIII-D has been used to investigate ELM suppression in plasmas with similar shapes and collisionalities to ITER [20, 32, 33], with suppression at collisionalities $\nu_c^* < 0.35$ but only mitigation above that. Experiments on MAST [34] using $n_{RMP} = 4$ and 6 have achieved mitigation, increasing f_{ELM} eightfold. KSTAR has seen, with $n_{RMP} = 1$, complete suppression of ELMs and also two distinct stages after RMP activation. First the plasma energy, toroidal rotation and density decrease by a small factor while the ELMs are being suppressed. Secondly, when ELMs are fully suppressed, these quantities plateau [35]. At AUG, similar discoveries have been made using $n_{RMP} = 2$ [30, 36] and, perhaps most importantly, strong mitigation was observed on JET under operation with an ITER-like wall (ILW) [37].

ITER's tungsten divertor introduces further requirements on ELM control [24], as W build up in the plasma core could cause catastrophic energy losses. Hence, additional methods to provide enhanced transport will need to be implemented, else low power ELMs must be allowed to occur to provide this enhancement. ELMs, however, are the main source of divertor impurities in the main plasma, so their suppression could itself be sufficient to bring core levels of W below the required threshold. Experiments on AUG found that in a type I ELM-mitigated regime the fraction of W in the plasma is lowered by a factor of 2 compared to in unmitigated regimes [30].

The magnitude of the field applied by RMP coils is 10^{-4}~10^{-3} T [38]. These relatively tiny perturbations disrupt the toroidal symmetry of the magnetic field, making it 3D rather than 2D. Field line paths become direction specific (clockwise path is different from the anti-clockwise path) and the edge flux surfaces are no longer smooth but instead exhibit lobe structures, especially in the X-point region. Visualisation of these lobes can be seen in figure 6, showing very good overlap between simulation and experimental data.

The X-point lobe patterns' radial length scales linearly with the magnitude of the applied RMP. They develop more complexity and size with increasing perturbation mode number [39]. More specifically, their size increases radially yet they have a smaller poloidal spread for increasing n_{RMP} [40]. These lobes pose a danger for the divertor plates: now the heat flux is 3D, their erosion will not be isotropic over the plates, causing roughening of the surface which will further enhance the heat load disparity. This separatrix splitting was first observed on MAST [41] and soon after on DIII-D [42]. RMP introduction also instigates slowing of the plasma rotation on DIII-D [19].

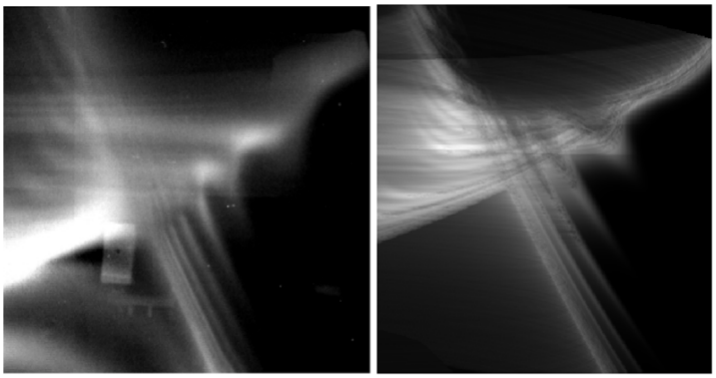

Figure 6: Camera image of $n_{RMP} = 6$ X-point lobes on MAST (left), ERGOS simulation for comparison (right) [39].

3.2 Pellet Injection

ASDEX Upgrade trialled the first usage of fuel pellet injection to trigger ELMs in 2003 [43]. Projectile pellets provoke type 1 ELMs when they penetrate into the pedestal [24].

Pellet injection is thought to provoke ELMs due to the fact that when a pellet enters the plasma it ablates, quite rapidly increasing the density in the small surrounding area of plasma. If the pellet has sufficient mass then this density increase will push the edge plasma parameters beyond the ballooning limit [44], causing an ELM with similar pathway to (ii) in figure 4. This can be cycled at frequencies at or above the natural ELM frequency to provide external control over these plasma eruptions. As this density increase is very localised, the toroidal mode number n of the ELMs produced is quite high in comparison to natural peeling-ballooning ELMs [44].

ELM magnitude scales as $f_{ELM}\Delta W_{ELM} \sim$ constant (equation 1) [16, 17, 24], so influencing factors which decrease the time between ELMs will consequently decrease their power. Sufficiently increasing f_{ELM} has the benefit of ensuring that no one single ELM will cause critical damage to the PFCs or the divertor;

however, high repetition rate thermal cycling of these first layer components may have severe long term impacts. Much research is under way to ascertain more precisely the thermal cycling tolerances of these components. Large networks of cracks can form in tungsten tiles after repeated exposure to type I ELM-like heat fluxes [45], which could be extremely detrimental to the extended operation of ITER.

As discussed in section 2, the ELM deposition area on the divertor scales with ELM energy. In ITER's testing phase the full extent of this relationship must be established in order to gauge how high it is beneficial to raise f_{ELM} by pellet pacing (or another triggering method). If said relationship was found to be very firm it will make these triggering methods redundant for ELM damage reduction [8].

Pellet triggering has been experimented with alongside gas injection ELM control on JET [46]. The gas injection controller was able to regain the target f_{ELM} within 0.5 s after some disturbance caused it to change. Parallel use of these control systems allowed more continued study of pellet injection triggering. Even when a pellet does not trigger an ELM, the gas injection keeps f_{ELM} at the required level, giving optimal fusion performance throughout the discharge as W impurities are continually flushed out [46].

A phenomenon known as trigger lag was seen on experiments on tokamaks with metal (W) walls, AUG-W and JET-ILW. This imposes a limit on the possible f_{ELM} that can be reached by pellet injection, as a pellet injected too soon after an ELM does not prompt an ELM. In previous campaigns on these machines, with non-metal carbon walls, trigger lag was not observed [44]. Additionally, in AUG-W, when nitrogen was injected into the divertor region the trigger lag time reduced by a factor of 5, to ~2 ms [44]. ELM triggering probability and its dependence on the time since the previous ELM and the pellet mass is shown in figure 7, showing that the time since the last ELM has a huge effect on the subsequent possibility of triggering and ELM.

Pellet injection on AUG shows that this lag time is unaffected by injection velocity or pellet mass, and instead is dependent on the current plasma scenario [48]. Triggering by this method has a wide range of success rates over different plasma scenarios. For instance, on AUG, ELM triggering is extremely successful when nitrogen gas is seeded in the divertor region [49]. However, this is unlikely to be viable on ITER when detachment at the divertor must be precisely controlled. More work is required to uncover the reasons behind the varying success of ELM triggering by

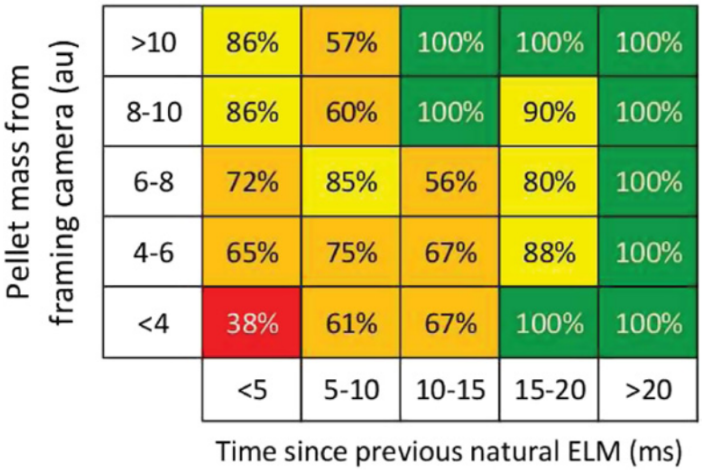

Figure 7: Efficiency of pellet ELM triggering on JET depending on the kick magnitude and the time since the last natural ELM [47].

pellet injection before its implementation on ITER.

The probability of triggering an ELM by injection of a given pellet heavily depends on the speed and mass of said pellet. Figure 8 shows the effect of pellet mass and injection speed on the efficiency of ELM triggering. Indicated by the arrow, a mass of 2.1×10^{20} a.u. is the threshold for guaranteeing a triggering instance at a reasonable range of speeds.

3.3 Vertical Kicks

Fractional shifts in the vertical position of the plasma, $\sim 1-3\%$ of the minor radius [24], executed rapidly, augment the edge current so as to potentially mitigate ELMs [50] by causing the instability to follow a similar path to (iii) in figure 4. NSTX [51] and KSTAR [52] produced results showing that the triggering of type I ELMs when the plasma is in upward motion (away from the X-point), while AUG [53] and JET [50] found that the precise opposite was more consistent at ELM triggering. The downwards preference for triggering was also observed on TCV [54], however for plasmas with type III ELM production tendencies.

Vertical kicks have the greatest effect on the position of the top and bottom of the edge plasma [51]. Figure 9, on NSTX, shows how the top edge plasma moves by up to 10 cm, while the center of the plasma moves approximately 4 cm and the bottom edge remained essentially stationary. The compression instigated by the kicks caused a minor, $< 2\%$, reduction in plasma volume on JET [50]. In addition, while the top edge plasma on JET moved a similar amount to that in NSTX, 7 cm, the bottom edge also moved, albeit a factor 3 shorter distance [50]. This disparity

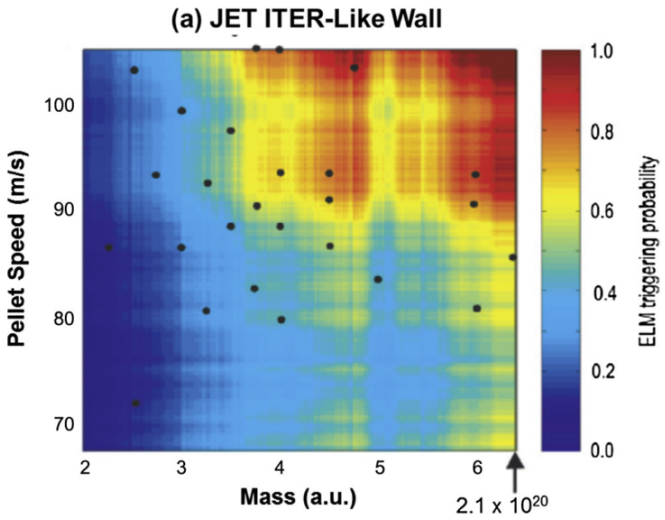

Figure 8: Efficiency of pellet ELM triggering on JET depending on the size of the pellet and its injection velocity [44].

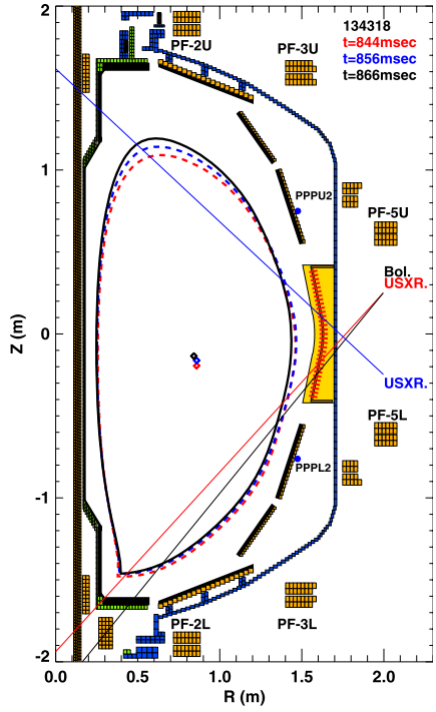

Figure 9: Cross-section of NSTX with plasma shapes at three intervals in the ELM control motion induced by the VS coils [51].

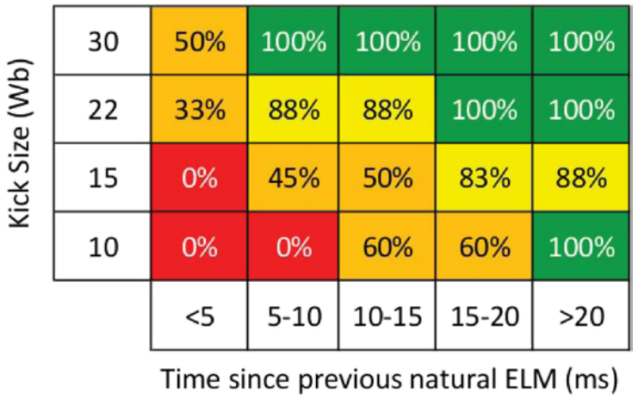

Figure 10: Efficiency of vertical kick ELM triggering on JET depending on the kick magnitude and the time since the last natural ELM [47].

is likely down to the different shaped devices, NSTX is a spherical tokamak, and the fact that JET's major radius is over 3 times larger, potentially making plasma motions more easily detected.

De la Luna *et al.* have shown the effectiveness of vertical kicks for ELM control on JET [50]. These experiments were conducted with the ILW in JET, which is the machine closest in size to ITER, to lower the complexity of extrapolation to operation on ITER, compared with other devices. A plot of triggering efficiency averaged over 150 kicks on JET can be seen in figure 10.

Figure 11 encapsulates the ability of vertical kicks to control ELM frequency. The kick frequency, f_{kick}, delivered first at 17 seconds was approximately equal to the natural ELM frequency of the plasma and this triggering had little to no effect on plasma properties, such as n_e. De la Luna *et al.* state that this shows that kicks change plasma parameters only via physical mechanisms directly linked to f_{ELM} increases [50]. Kicks implemented on KSTAR had a ~25 mm amplitude, about 5% of its minor radius (0.5 m [55]), at 50 Hz and triggered ELMs almost precisely as the plasma reached peak velocity [52].

ELM triggering by vertical kicks can be used to lower plasma core impurity levels, which may be useful in shot sections with higher chances of W build-up in ITER. A key advantage of vertical kicks over pellet pacing is that there is no unwanted density increase for vertical kicks, whereas too much pellet injection can negatively affect the plasma. Additionally, vertical kicks can be utilised in any part of a discharge, unlike RMP control because it is a resonant effect [50].

With the JET ILW, ELM triggering by vertical kick was very successful and sturdy over a wide range of

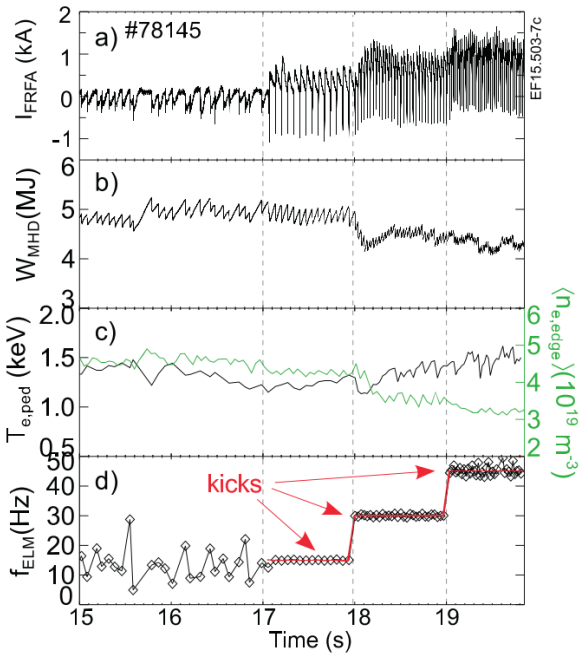

Figure 11: Visualisation of ELM frequency locking to the vertical plasma motion caused by vertical kicks. Panel (a) shows the VS coil current, (b) measured stored energy, (c) the average edge n_e (green) and the pedestal temperature (black) and (d) f_{ELM}, the ELM frequency with the vertical kick frequency indicated by the red arrows [50].

operating criteria; most critically, regimented triggering was seen over a large window of pedestal collisionalities ($\nu_e^* \sim 0.2 - 0.6$) [50]. The same JET team also found that the plasma parameters heavily influenced the threshold vertical kick magnitude required to prompt an ELM.

3.4 How these methods will work on ITER

ITER will utilise at least two major ELM control systems, RMP coils and pellet injectors [56]. Figure 12 shows the planned positions of the ELM control coils in ITER.

In order to counteract the uneven divertor heat loads due to the flux surface lobes produced by the RMP coils, the perturbations will be rotated toroidally above 1 Hz [26] so as to smear out the deleterious effects over the whole divertor. Alternatively the toroidal mode number of the perturbation could be cycled. Different edge perturbations investigated on MAST, $n_{RMP} = 2, 3, 4$ and 6, found that the footprint at the divertor changed for each value of n_{RMP} [40]. The problem with this partial solution is that cycling could damage the RMP coils in the long term [24]. This is very undesirable as they are within the

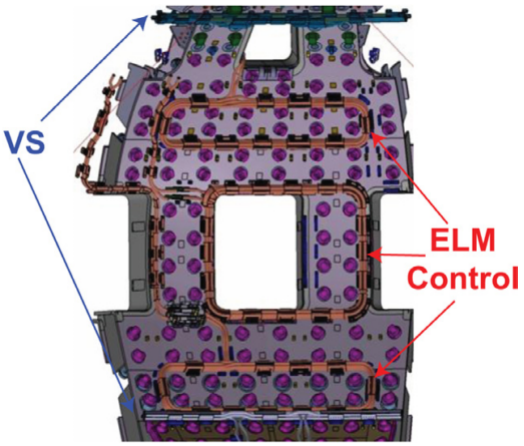

Figure 12: RMP (ELM control) and vertical stability (VS) coil layout on one ninth of the ITER outboard vessel wall [8].

first vacuum wall and so cannot be replaced easily.

Currently, ITER is expected to use $n_{RMP} = 3$ and 4 [40]. A decision made after the success on DIII-D of complete suppression, in similar conditions to the ITER baseline scenario, using $n_{RMP} = 3$ in 2008 [20, 57]. The understanding of this suppression was more recently advanced by Wade *et al.* [58]. The group found that it is the alignment of the $n = 3$ rational surface with zero perpendicular electron velocity ($\omega_{\perp e} = 0$) and the pedestal peak that is critical in achieving suppression. Regarding the requirement $\omega_{\perp e} = 0$, it was found necessary to apply neutral beam injection (NBI) with the plasma rotation, as anti-rotation application does not produce a $\omega_{\perp e} = 0$ region, preventing ELM suppression altogether [58].

Snyder *et al.* have proposed a mechanism for RMP induced suppression [59], in which a stochastic [1] region or layer of resonant magnetic islands form due to the RMP penetration of the edge plasma. This enhances the rate of edge transport which ensures the edge pressure and current density remain below the peeling-ballooning boundary.

Edge safety factor, q_{95} - safety factor at 95% poloidal flux, imposes strict boundaries on suppression on DIII-D. ELM suppression is only seen for $3.32 < q_{95} < 3.67$ [57], which poses issues as the expected value is around $q_{95} = 3$ in the default ITER scenario [60]. This "q-window" in which suppression occurs is less wide for ITER similar shaped (ISS) plasmas than for plasma shapes with lower triangularity [20].

The explanation [59] of RMP suppression also

[1] having a random probability distribution

provides potential answer for the existance of these "q-windows". Positioning of the edge safety factor q_{95} dictates the location of the resonant island chain or stochastic layer. If this is situated in a select region, within the pressure-current ELM recovery path, it will prevent a crash. For q_{95} values outside of this window, this chain or layer will either be too deep in the plasma, allowing ELMs to occur, or too close to the edge and thus not effective as it is blocked by the plasma response [59]. Plasma response to RMP activation is discussed in [61].

Due to the wide variation of ELM triggering success with pellet injection, significant further study is required regarding the potential for ELM control using this method in different regimes on ITER. The disparity in the accomplishments of the technique when operating with carbon walls versus metal walls calls into question pellet injection's potential usefulness on ITER. If pellet injection can only bring f_{ELM} above the required PFC and divertor damage threshold in certain scenarios, then ITER may be left with a severely curtailed domain of operation. However, the localised benefits of pellet triggering will no doubt be useful. Overall plant efficiency could be increased if pellet injection can serve a double purpose of ELM triggering and refuelling; it is estimated that 40% of the refuelling requirements of ITER can be provided by pellets used for ELM control [22], potentially allowing, in future, the complete coalescing of these two vital components of plasma control. The close alignment of results from AUG and JET, with metal walls, provides hope for the success of pellet injection on ELM triggering for ITER [62].

By selecting not just the ideal pellet mass but also the optimal injection point, the heat flux incident on the divertor can be brought to an optimised minimum [44].

Vertical stability coils may be implemented as a fall back ELM control method [22]. VS coils were already included into the design, just not initially for ELM triggering (they have been used in most tokamaks already for tweaking purposes prior to the realisation that they can be used to control ELMs). De la Luna *et al.* expects that vertical kicks will be a promising method of ELM control for ITER [50]. Furthermore, the same group found that there is a threshold to the vertical motion traversed by the plasma to produce an ELM. This threshold distance is reduced for lower edge collisionalities and higher pedestal temperatures. Given that ITER will operate in H-mode at quite high temperature and relatively low collisionality this is promising for its ELM control process. The shorter the distance the plasma is forced to move, the more rapidly the motion can be repeated and the lower the chance is of causing consequential instabilities (such as destabilising core modes).

The fact that VKs do not utilise any resonant effect in triggering ELMs means that they can be applied at any time throughout a shot [47]. This is especially useful in temporal regions when the $q-$profile is evolving or in the initial current ramping phase. Another benefit of VKs is that they can be used in plasmas with high helium content (minimal evidence of the effectiveness of pellet pacing in these conditions exists) [47]; this may be useful in the later stages of shots on ITER.

4 Alternative modes of operation

Quiescent H-mode (QH-mode) retains the benefits of the central pedestal without the cyclic energy losses by ELMs, which are damaging to both fusion performance and the device's components. It has been attained on several tokamaks; namely DIII-D, JET and ASDEX-U [63, 64], and is a potentially promising operating regime for ITER if enough prior research and solid extrapolation can be performed.

The I-mode is an operating regime that combines the desirable elements of H- and L-mode [65] and has automatic ELM suppression [66]. It is more easily available to higher-field machines and has been investigated most considerably on Alcator C-Mod. Core impurity levels are lowered in I-mode as it lacks an edge particle transport barrier, while retaining the edge energy transport barrier. Hence, I-mode can be distinguished by observing an H-mode like temperature pedestal along with an L-mode like density profile [65].

5 Necessary future work

Before the first plasma run in ITER, it must be able to operate in a regime with strictly controlled ELMs in order to ensure a reasonable lifetime of the machine. More work is required to build a stronger physical basis of suppression and mitigation in ITER-like scenarios, building from DIII-D [20, 32] and JET [37] experiments, such that more realistic extrapolations can be drawn regarding the potential success of these control techniques on ITER.

Alongside the development of the optimal RMP mode to apply in ITER's different regimes, there must be continual assessment of the projected lifetimes of

the ELM control coils. Provisions need to be made for the worst case scenario in which several coils fail quickly: a protocol of which perturbations are conducted depending on the arrangement of the remaining coils.

Pellet injection has the potential to provide sufficient mitigation for ITER in all sections of a discharge [44]. However, more work is needed to gain a better understanding of the mechanisms behind ELM triggering by pellet injection. More specifically, in depth knowledge is required in order to accurately predict the results of pellet injection over the whole range of ITER's operating regimes. The efficiency saving of combination of refuelling and pellet triggering techniques may not be fully understood prior to ITER and will have to be assessed during the early phases of it's operation [44].

Vertical kick usage can produce mitigated ELM scenarios alongside controlling accumulation of core plasma impurities [50]. Another positive of VKs is the fact that they can be carried out with existing hardware on ITER: vertical stability coils have been included in the design since before it was realised that VKs could be used for ELM control. Additional experiments must be undertaken to build a more solid basis regarding the triggering mechanism that VKs take advantage of. Once the underlying physics is better understood, more solid predictions for their operation on ITER can be made [50].

To summarise, the ELM suppression and mitigation techniques discussed in this paper require further investigation before they can be reliably implemented on ITER. The basis for the necessary hardware's inclusion into the physical structure has been achieved and much of the evidence collected in this review is compelling in view of the success of these ELM control techniques in keeping ITER operational for as long as possible.

Each of the three ELM control methods reviewed have positives and negatives, and overall complement each other rather well. RMP control will likely be employed the most frequently, as it has the potential to provide complete suppression of ELMs - which is the most desirable regime for ITER. Pellet injection and vertical kick mitigation techniques both have their own useful domains in ITER's operation, mainly in discharge sections in which resonant effects cannot be used. It is expected that an optimised configuration of these three techniques will provide ample opportunity for ELM control on ITER, allowing higher records to be set in fusion performance.

References

[1] M. Keilhacker et al. *Plasma Physics and Controlled Fusion* 25.1A (1984), pp. 49–63.

[2] F. Wagner. *Plasma Physics and Controlled Fusion* 49.12B (2007), pp. 1–33.

[3] H. Zohm. *Plasma Physics and Controlled Fusion* 38.2 (1996), pp. 105–128.

[4] P.B. Snyder et al. *Physics of Plasmas* 9.5 (2002), pp. 2037–2043.

[5] H.R. Wilson et al. *Physics of Plasmas* 9.4 (2002), p. 1277.

[6] P.B. Snyder et al. *Nuclear Fusion* 49.8 (2009), p. 085035.

[7] H.R. Wilson and S. C. Cowley. *Physical Review Letters* 92.17 (2004), pp. 175006–1.

[8] P.T. Lang et al. *Nuclear Fusion* 53.4 (2013), p. 043004.

[9] D.N. Hill. *Journal of Nuclear Materials* 241-243 (1997), pp. 182–198.

[10] C.P. Perez et al. *Plasma Physics and Controlled Fusion* 46.1 (2004), pp. 61–87.

[11] M.R. Wade. *Fusion Engineering and Design* 84.2-6 (2009), pp. 178–185.

[12] P.B. Snyder et al. *Plasma Physics and Controlled Fusion* 46.5A (2004), A131–A141.

[13] H. R. Wilson et al. *Plasma Physics and Controlled Fusion* 48 (2006), A71–A84.

[14] J. W. Connor et al. *AIP Conference Proceedings* 1013 (2008), pp. 174–190.

[15] T. Eich et al. *Journal of Nuclear Materials* 363-365.1-3 (2007), pp. 989–993.

[16] A.W. Leonard et al. *Journal of Nuclear Materials* 266 (1999), pp. 109–117.

[17] A. Loarte et al. *Plasma Physics and Controlled Fusion* 44.9 (2002), pp. 1815–1844.

[18] T. Eich et al. *Nuclear Fusion* 53.9 (2013), p. 093031.

[19] A. Kirk et al. *Physical Review Letters* 108.25 (2013), p. 32.

[20] T.E. Evans et al. *Nuclear Fusion* 48.2 (2008), p. 10.

[21] J.W Connor et al. *Nuclear Fusion* 44.4 (2004), R1–R49.

[22] A. Loarte et al. *Nuclear Fusion* 54.3 (2014), p. 033007.

[23] G. Federici, A. Loarte and G Strohmayer. *Plasma Physics and Controlled Fusion* 45.9 (2003), pp. 1523–1547.

[24] Fusion Frontiers Lectures. A. Kirk. 2016.

[25] A. Loarte et al. *Plasma Physics and Controlled Fusion* 45.9 (2003), pp. 1549–1569.

[26] A. Loarte. Tech. rep. ITER, 2013.

[27] ORNL PMIF-PFC. E. Tsitrone. 2013.

[28] T. Eich et al. *Journal of Nuclear Materials* 415.1 SUPPL (2011), S856–S859.

[29] A. Loarte 11-16 October 2010, Daejeon, Republic of Korea. www-naweb.iaea.org/napc/physics/FEC/FEC2010.

[30] W. Suttrop et al. *Physical Review Letters* 106.22 (2011), pp. 1–4.

[31] P.T. Lang et al. *Nuclear Fusion* 52.2 (2012), p. 023017.

[32] M.J. Lanctot et al. *Nuclear Fusion* 53.8 (2013), p. 9.

[33] S. Mordijck et al. *Plasma Physics and Controlled Fusion* 53.12 (2011), p. 122001.

[34] A. Kirk et al. *Nuclear Fusion* 53.4 (2013), p. 043007. arXiv: 1305.3723.

[35] J. Kwak et al. *Nuclear Fusion* 53.10 (2013), p. 104005.

[36] R. Fischer et al. *Plasma Physics and Controlled Fusion* 54.11 (2012), p. 115008.

[37] Y. Liang et al. *Nuclear Fusion* 53.7 (2013), p. 9.

[38] T.E. Evans. *Plasma Physics and Controlled Fusion* 57.12 (2015), p. 123001.

[39] J.R. Harrison et al. *Nuclear Fusion* 54.6 (2014), p. 064015.

[40] I.T. Chapman, M. Becoulet and T. Bird. *Nuclear Fusion* 54.083006 (2014).

[41] A. Kirk et al. *Physical Review Letters* 108.25 (2012), pp. 1–4.

[42] M.W. Shafer et al. *Nuclear Fusion* 52.12 (2012), p. 122001.

[43] P.T. Lang et al. *Nuclear Fusion* 43.10 (2003), pp. 1110–1120.

[44] L.R. Baylor et al. *Journal of Nuclear Materials* 463 (2015), pp. 104–108.

[45] J. Linke et al. *Nuclear Fusion* 51.7 (2011), p. 073017.

[46] M. Lennholm et al. *Nuclear Fusion* 55.6 (2015), p. 063004.

[47] I. T. Chapman et al. *Plasma Physics and Controlled Fusion* 58.1 (2016), p. 14017.

[48] P.T. Lang et al. *Nuclear Fusion* 54.8 (2014), p. 83009.

[49] A. Kallenbach et al. *Nuclear Fusion* 52.12 (2012), p. 122003.

[50] E. de la Luna et al. *Nuclear Fusion* 56.2 (2016), p. 026001.

[51] S.P. Gerhardt et al. *Nuclear Fusion* 50.6 (2010), p. 064015.

[52] J. Kim et al. *Nuclear Fusion* 52.11 (2012), p. 114011.

[53] P.T. Lang et al. *Plasma Physics and Controlled Fusion* 46.11 (2004), pp. L31–L39.

[54] A.W. Degeling et al. *Plasma Physics and Controlled Fusion* 45.9 (2003), pp. 1637–1655.

[55] D.I. Choi et al. *17th Ieee/Npss Symposium on Fusion Engineering, Vols 1 and 2* June 1997 (1998), 215–220\r1156.

[56] A. Loarte. October. 2010, pp. 545–546.

[57] M.E. Fenstermacher et al. *Physics of Plasmas* 15.5 (2008).

[58] M.R. Wade et al. *Nuclear Fusion* 55.2 (2015), p. 23002.

[59] P.B. Snyder et al. *Physics of Plasmas* 19.5 (2012).

[60] C. Gormezano et al. *Nuclear Fusion* 47 (2007), S285–S336.

[61] F.L. Waelbroeck. *Nuclear Fusion* 49.10 (2009), p. 104025.

[62] P.T. Lang et al. *Plasma Physics and Controlled Fusion* 57.4 (2015), p. 045011.

[63] K.H. Burrell et al. *Plasma Physics and Controlled Fusion* 44.A (2002), pp. 253–263.

[64] W. Suttrop et al. *Nuclear Fusion* 45.7 (2005), pp. 721–730.

[65] D.G. Whyte et al. *Nuclear Fusion* 50.10 (2010), p. 105005.

[66] E.S. Marmar et al. *Nuclear Fusion* 55.10 (2015), p. 104020.